Published in final edited form as:
Dev Cell. 2008 November ; 15(5): 691–703. doi:10.1016/j.devcel.2008.09.017.

Chronophin mediates an ATP-sensing mechanism for cofilin dephosphorylation and neuronal cofilin-actin rod formation

Timothy Y. Huang[1], **Laurie S. Minamide**[2], **James R. Bamburg**[2], and **Gary M. Bokoch**[1]

1*Department of Immunology and Microbial Science, Department of Cell Biology, The Scripps Research Institute, IMM14, 10550 N. Torrey Pines Rd., La Jolla CA 92122 USA*

2*Department of Biochemistry and Molecular Biology, Colorado State University, Fort Collins, CO 80523 USA*

Summary

Actin and its key regulatory component cofilin are found together in large rod-shaped assemblies in neurons subjected to energy stress. Such inclusions are also enriched in Alzheimer's disease brain, and appear in transgenic models of neurodegeneration. Neuronal insults such as energy loss and/or oxidative stress result in rapid dephosphorylation of the cellular cofilin pool prior to its assembly into rod-shaped inclusions. Although these events implicate a role for phosphatases in cofilin rod formation, a mechanism linking energy stress, phosphocofilin turnover and subsequent rod assembly has been elusive. Here, we demonstrate the ATP-sensitive interaction of the cofilin phosphatase Chronophin (CIN) with the chaperone Hsp90 to form a biosensor that mediates cofilin/actin rod formation. Our results suggest a model whereby attenuated interactions between CIN and Hsp90 during ATP depletion enhance CIN-dependent cofilin dephosphorylation and consequent rod assembly, thereby providing a mechanism for the formation of pathological actin/cofilin aggregates during neurodegenerative energy flux.

Keywords

Cofilin dephosphorylation; Cofilin rods; ATP depletion; Neurodegeneration; Hsp90; Chronophin; Neurons; Actin

Introduction

The cyclical exchange between actin monomers and its assembly into filaments is an energy-dependent process, where the incorporation of ATP-actin into filaments (F-actin) ultimately results in ATP-hydrolysis (Pollard and Borisy, 2003). Recycling factors such as cofilin and related ADF (Actin Depolymerizing Factor) family members bind ADP-actin filaments to promote P_i release and filament severing (Carlier et al., 1997; Ichetovkin et al., 2002; Pollard and Borisy, 2003). Filament severing accelerates the dynamic exchange of actin between monomers and filaments by simultaneously stimulating actin filament disassembly (Carlier et al., 1997) and promoting actin polymerization on newly-severed barbed ends (Ichetovkin et

Correspondence to: E-mail: bokoch@scripps.edu.

al., 2002). Due to the abundance of cellular actin, the ATP expenditure associated with each round of actin polymerization and depolymerization is energetically costly. Indeed, inhibiting actin turnover during anoxic stress in neurons attenuates ATP depletion by as much as 50% (Bernstein and Bamburg, 2003).

Since limiting actin dynamics under energy-depleted conditions would allow cells to retain ATP consumed by a cycling actin population, a cellular mechanism to inhibit actin cycling in response to ATP-stress would be beneficial to cell types sensitive to energy drain. Interestingly, cofilin is rapidly reorganized together with actin into large rod-shaped inclusions in neurons during ATP depletion (Minamide et al., 2000), thereby presenting a mechanism for immobilizing cofilin/actin complexes and attenuating cofilin-driven actin treadmilling. In support of this, generation of cofilin/actin rods in rat hippocampal neurons can slow ATP decline during anoxic stress (Bernstein et al., 2006). Formation of such inclusions may also contribute to synaptic defects associated with ischemic brain injury (e.g. stroke) (Maloney and Bamburg, 2007).

The persistence of cofilin/actin rods can have dramatic long-term detrimental effects on neuronal function. For example, rod formation in *Aplysia* neurons reduced synaptic strength and impaired long-term facilitation elicited by 5-hydroxytryptamine in sensory-to-motor synapses (Jang et al., 2005). Rods also block transport of vesicles containing amyloid precursor protein (APP) and enzymes involved in processing amyloid β, causing the accumulation of APP at rods in neurons (Maloney et al., 2005).

ADF/cofilin interactions with actin are greatly enhanced through their dephosphorylation at Ser-3 (Agnew et al., 1995). During ATP depletion, cofilin characteristically exhibits rapid dephosphorylation prior to co-assembly with actin into rods (Minamide et al., 2000), suggesting that a cofilin phosphatase may link phosphocofilin turnover to rod formation. Here, we demonstrate an ATP-sensitive regulatory mechanism for the cofilin phosphatase Chronophin (CIN), a haloacid dehalogenase (HAD)-family phosphatase abundantly expressed in brain (Gohla et al., 2005), in mediating neuronal cofilin dephosphorylation and rod formation.

Results

CIN binds Hsp90

GST-CIN expressed in HeLa cells consistently co-precipitated an endogenous ~90kDa band which was absent in the GST control (Figure 1A). This component was identified as Hsp90β by mass spectrometric analysis, and the association between GST-CIN and Hsp90β in glutathione-Sepharose precipitates was confirmed by immunoblot analysis (Figure 1B). Under these conditions we failed to observe interactions between Hsp90 and GST alone, or with the cofilin phosphatase Slingshot (GST-SSH-1L) (Niwa et al., 2002) (Figure 1B). To verify this interaction, his_6myc-CIN complexes were precipitated and eluted using Ni-chelate resin from lysates derived from a clonal HeLa cell line stably expressing his_6myc-CIN (hmc2–3) at levels slightly above endogenous CIN levels (Figure 1C). Although we detected Hsp90 in his_6myc-CIN elution fractions derived from hmc2–3 lysates, we observed little or no Hsp90 elution in non-expressing control cell lysates.

To establish whether Hsp90 interacted directly with CIN, we transferred GST-purified CIN, GST alone, or the Hsp90 co-chaperone Aha1 onto nitrocellulose and performed a far-western overlay with purified Hsp90 (Figure 1D). Using this method, we observed direct Hsp90 interaction with GST-CIN and Aha1, but not with GST alone. The effects of the Hsp90 interaction on CIN phosphatase activity was investigated using purified recombinant Hsp90 in an *in vitro* CIN-dependent cofilin dephosphorylation assay. While we could detect cofilin

dephosphorylation in GST-CIN precipitates, the addition of Hsp90 attenuated CIN-dependent cofilin dephosphorylation (Figure 1E), indicating that Hsp90 has inhibitory effects on CIN activity.

ATP enhances CIN/Hsp90 interaction

Hsp90 ATP-binding and hydrolysis has been shown to be an important aspect of Hsp90 function as a cellular chaperone *in vivo* (Obermann et al., 1998; Panaretou et al., 1998). Pharmacological Hsp90 inhibitors such as geldanamycin competitively bind the Hsp90 ATP-binding pocket (Grenert et al., 1997), and disrupt its association with client substrates (Pearl and Prodromou, 2006), illustrating the importance of ATP-loading in the association of Hsp90 with its substrates. To determine whether ATP affects CIN/Hsp90 interactions *in vitro*, we assayed the ability of GST-CIN beads to co-precipitate with recombinant Hsp90 in the presence or absence of various nucleotides. We observed that ATP consistently enhanced co-precipitation of Hsp90 with CIN (Figure 2A), suggesting that the abundance of Hsp90/CIN complexes may be affected by nucleotide availability. ADP enhanced Hsp90/CIN interactions to some extent compared to ATP-free samples in our assays, but these effects were weak compared with ATP (Figure 2A). There was little effect of other nucleotides (AMP or the non-hydrolyzable analogue ATPγS) on the Hsp90/CIN interaction (Figure 2A). This closely reflects previous results demonstrating the ATP-enhanced interaction between Hsp90 and the progesterone receptor, with little effect using ADP and AMP-PNP (Smith et al., 1992). As in our initial co-elution experiments with GST-CIN (Figure 1A), silver staining of GST-CIN/recombinant Hsp90 complexes revealed that ATP only induced Hsp90 co-precipitation with a fraction of GST-CIN (Figure S1A).

Using an affinity-purified CIN polyclonal antibody, we were consistently unable to co-immunoprecipitate endogenous CIN together with Hsp90 from bovine brain lysates. Since preparation of cell lysates under ATP-free conditions may largely attenuate CIN/Hsp90 interactions, we tested whether addition of ATP could restore CIN/Hsp90 binding. Indeed, we found that addition of 5mM ATP enabled Hsp90 co-immunoprecipitation using CIN antibodies, while no Hsp90 was detected using control antibodies (Figure 2B).

To determine whether ATP had an effect on enhancing CIN/Hsp90 interactions *in vivo*, we assessed the effects of ATP depletion on his_6myc-CIN/Hsp90 co-precipitation from clonal his_6myc-CIN expressors using an inhibitor of oxidative respiration (antimycin A). Immunoblots of elution fractions from NiNTA precipitates revealed reduced co-elution of his_6myc-CIN with Hsp90 after ATP depletion (Figure 2B), supporting the notion that ATP may be required for CIN/Hsp90 interaction. Quantitative analytical immunoblotting revealed that 19 ng of Hsp90 co-eluted with 160 ng of CIN in pooled peak co-eluates (Figure S1B and C). Thus, about 7% (after adjusting for molecular weight) of CIN was bound to Hsp90 under these conditions. However, this is likely to be an underestimate, as our co-immunoprecipitation experiments indicate that CIN/Hsp90 complexes are lost during lysis and precipitation under ATP-free conditions.

We next examined whether the exposure of cells to the Hsp90 inhibitor 17AAG (17-(allylamino)-17-demethoxygeldanamycin, a geldanamycin derivative) had effects on Hsp90/CIN interactions. The presence of 17AAG also attenuated Hsp90/CIN co-elution in NiNTA agarose precipitates to a similar extent as observed with energy depletion (Figure S1D). Together, these observations indicate that depletion of ATP, or competitive inhibition of Hsp90 ATP-loading (using 17AAG), can decrease the formation of Hsp90/CIN complexes.

ATP and Hsp90 regulate CIN activity

Our results suggest that interactions between Hsp90 and CIN are sensitive to energy flux, and imply that depletion of ATP may stimulate phosphocofilin turnover through the attenuation of Hsp90/CIN complexes. Cofilin dephosphorylation triggered by energy depletion should therefore be sensitive to cellular CIN protein levels. To test this hypothesis, we varied CIN levels in HeLa cells by overexpression or siRNA-mediated depletion, and measured the disappearance of phosphocofilin. Overexpression of CIN accelerated cofilin dephosphorylation during ATP depletion (Figure 3A): normalized p-cofilin levels 5 and 10 min post-ATP depletion were lower in CIN-expressing cells compared to the vector control. Conversely, siRNA-mediated CIN depletion attenuated p-cofilin dephosphorylation 5 to 10 min post-ATP depletion compared to the siRNA control (Figure 3B). Interestingly, CIN overexpression or siRNA depletion had only limited effects on steady-state phosphocofilin levels under unperturbed conditions (0 timepoint, Figures 3A,B), indicating that CIN activity may be tightly regulated, as suggested previously (Gohla et al., 2005).

We were also interested in determining whether perturbation of the cofilin phosphatase SSH could produce comparable effects in modulating phosphocofilin levels during ATP depletion. Similar to CIN depletion, we observed that siRNA-mediated SSH-1L knockdown results in delayed phosphocofilin turnover (5 to 10 min.) following ATP depletion (Figure S2A and B). However, comparison of normalized phosphocofilin levels under steady state conditions revealed that, while CIN depletion has very little effect on cofilin phosphorylation, SSH knockdown consistently produces a significant increase in phosphocofilin (Figure S2C), indicating that sustained phosphocofilin pools during anoxic treatment are derived, at least in part, from elevated p-cofilin levels prior to ATP depletion. This further suggests that while SSH moderates the phosphocofilin milieu under unperturbed conditions, CIN activity may be reserved for more specialized circumstances such as cell division (Gohla et al., 2005) and energy stress.

Since these observations indicate that CIN activity may be rapidly induced upon ATP depletion, we measured CIN phosphatase activity during anoxic stress: HeLa cells transfected with either GST or GST-CIN expression constructs and were subjected to ATP depletion. GST proteins were then isolated, and cofilin dephosphorylation measured *in vitro* using purified phosphocofilin (Figure S3). CIN precipitates demonstrated enhanced cofilin dephosphorylation after ATP depletion (Figure S3), indicating that CIN activity is indeed enhanced by ATP stress.

Overexpression of SSH-1L resulted in complete phosphocofilin turnover throughout the entire ATP depletion timecourse (Figure S4A), thereby giving little indication to the activation state of SSH during energetic stress. We therefore assayed SSH-GST precipitates during an ATP depletion timecourse for cofilin dephosphorylation (Figure S4B). Interestingly, we found that SSH activity was diminished after 10 and 30 min. of energetic depletion (Figure S4B). Since SSH activity is still quite robust 30 min. following ATP depletion, it remains possible that SSH can contribute to phosphocofilin turnover during energy stress.

To determine the involvement of Hsp90 in ATP-dependent phosphocofilin turnover *in vivo*, we assayed the effects of specifically inhibiting Hsp90 ATP-loading with 17AAG on steady state phosphocofilin levels. Similar to our observations with anoxic stress, we found that 17AAG induced potent cofilin dephosphorylation, where 80% of the cofilin pool is dephosphorylated over the vehicle (DMSO) control (Figure 3C). We consistently observed a strong attenuation of 17AAG-mediated phosphocofilin turnover upon CIN knockdown (Figure 3D), indicating that cofilin dephosphorylation mediated by Hsp90 inhibition is dependent on CIN. The addition of 17AAG with recombinant Hsp90 failed to abrogate Hsp90-dependent inhibition of CIN phosphatase activity *in vitro* (Figure S5A). This supports the notion that

17AAG triggers p-cofilin turnover *in vivo* through competitive effects on Hsp90 ATP-loading, and would therefore show little effect on purified Hsp90 *in vitro* under ATP-free conditions. Application of 17AAG did not affect cellular CIN levels (Supplemental Figure S5B), indicating that the effects of 17AAG are mediated primarily through effects on the Hsp90/CIN interaction.

CIN mediates cofilin rod assembly

Cofilin dephosphorylation appears to be prerequisite to its assembly into rod-shaped inclusions since phosphomimetic S3E cofilin constructs are unable to accumulate in rods (Jang et al., 2005), whereas wild-type or S3A cofilin constructs readily localize to rods (Minamide et al., 2000). Since our observations suggest that CIN mediates cofilin dephosphorylation during ATP-loss, we examined whether this energy-dependent switch mechanism could regulate the formation of cellular cofilin rods. Endogenous cofilin levels in HeLa cells are insufficient to induce rod formation during anoxic stress (Figure S6A). We therefore moderately elevated the cellular cofilin pool by stable expression of cofilin-GFP in a clonal HeLa cell line. Cofilin-GFP is normally distributed throughout the entirety of these cells, and application of ATP-depleting agents such as antimycin A and NaN_3/2-deoxyglucose results in the rapid aggregation (within 30 min) of cofilin-GFP into rod-shaped aggregates (Movie S1, Figure 4A). Approximately 80% of cells form cofilin-GFP rods after 30 min of ATP depletion (Figure 4B), correlating with the dephosphorylation of both endogenous cofilin and cofilin-GFP (Figure 4C).

The induction of cofilin-GFP rods by ATP depletion in our model system was quite homogenous, with most of the cell population forming rods at nearly identical rates (Movie S1). The synchrony of rod formation enabled us to assess whether perturbation of CIN levels affected rates of cofilin rod formation. CIN-targeting (or non-targeting) small RNA hairpins (shRNAs) and mRFP were co-expressed from separate loci on a single vector, thereby allowing us to tag shRNA-expressing cells (Figure 4D). Two differing CIN-targeting shRNA vector constructs (CIN1 and CIN4, as in Methods) were used, both of which reduced cellular CIN levels (Figure 4E). CIN-depleted cofilin-GFP expressing cells were co-cultured with non-transfected cells and rates of cofilin rod-formation were compared between shRNA-expressing (mRFP-tagged) and neighboring non-transfected cells during ATP depletion (Movie S2 and Movie S3). We found that cells transfected with non-targeting shRNA sequences or empty RFP vectors showed little difference in the rate of cofilin rod formation compared to co-cultured non-transfected cells (Movie S2), whereas there was a marked delay in cofilin rod formation in cells expressing CIN-targeting shRNAs (Figure 4F, Movie S3). By scoring percentages of transfected cells exhibiting delayed rod formation, we found that non-targeting controls had little effect to delay rod formation (NT, H1 vectors), while both CIN-targeting shRNA constructs delayed cofilin rod formation in a significantly higher percentage of cells (Figure 4G). We confirmed these results by transfecting synthetic siRNA CIN-targeting oligos into cofilin-GFP cells and tabulating proportions of rod-forming cells at various ATP depletion timepoints (Figure S6B). We consistently observed fewer rod-forming cells at intermediary timepoints (Figure S6B), indicating that knockdown of CIN protein levels caused a delayed rod-forming response.

Since ATP depletion could induce a robust rod-forming response, we examined if specific inhibition of ATP-dependent Hsp90 function was also involved in cofilin rod assembly. As Hsp90 inhibition with 17AAG resulted in a dramatic decrease in steady-state phosphocofilin levels, we hypothesized that 17AAG would also trigger cofilin rod formation. Indeed, a significant proportion of cofilin-GFP cells formed cofilin rods (27%) after 8 hours of 17AAG treatment (Figure 5A), suggesting that specific inhibition of Hsp90 ATP-loading can induce cofilin rod formation. We used two synthetic CIN siRNA oligos to deplete CIN in our model system (Figure 5B) and examined their effects on rod formation in combination with 17AAG.

We observed a striking reduction in the proportion of rod-forming cells with CIN depletion in the presence of 17AAG (Figure 5C), indicating that Hsp90-dependent rod formation occurs in a CIN-dependent manner.

Having established a requirement for CIN in cofilin rod formation in our model cell system, we investigated whether actin/cofilin rod formation in cultured primary neurons was also CIN-dependent. ATP depletion in murine hippocampal and cortical neuronal cultures resulted in the robust formation of numerous tapered cofilin rods (Figure 6A). In order to assay the effects of CIN perturbation on cofilin phosphoregulation and rod formation in primary neurons, we established a method to deplete murine CIN using synthetic siRNA oligos (Figure 6B, see Methods). Similar to our observations in the HeLa cell system, CIN depletion in cortical neurons results in a delay in phosphocofilin turnover during ATP depletion (Figure 6C), and suppresses the number of rod-forming hippocampal neurons up to 45 min. following ATP depletion (Figure 6D). Although most of the p-cofilin pool has been dephosphorylated 20 min. following ATP depletion, rod-forming hippocampal neurons peak in abundance by 30 min. (Figure 6D, Left graph), suggesting an apparent lag between cofilin dephosphorylation and peak rod formation. By counting the number of rods indexed over cell number (cofilin rod index), we observe that cofilin rod formation also peaks 30 min. after anoxic treatment (Figure 6D, Right graph). CIN depletion has maximal effects on suppressing the population of rod-forming cells and cofilin rod index 30 min. following ATP depletion (Figure 6D). These results indicate that while cofilin rod-producing cells in both the model HeLa system and primary neurons peak after 30 min. of ATP depletion, CIN depletion has maximal effects on cofilin rod formation at earlier timepoints in our cofilin-GFP HeLa model (10 to 20 min., Figure S6B) compared to 30 min. in primary neurons (Figure 6D). Indeed, siRNA-mediated CIN depletion significantly reduced both the abundance of rods (rod index) and overall percentage of rod-forming hippocampal neurons 30 min. following ATP depletion (Figure 6E).

Cofilin rod formation has been shown to be a fully-reversible phenomenon, where the repletion of neuronal cultures following anoxic stress results in the rapid dissolution of cofilin rods (Minamide et al., 2000). Similarly, we find that repletion of cofilin-GFP-expressing HeLa cells results in the dissolution of cofilin-GFP rods (Movie S4) and rephosphorylation of cofilin (Figure S7A). Long-term recovery following ATP depletion, however, also results in the reformation of cofilin rods in a proportion of cultured neurons (persistent rods) (Minamide et al., 2000), suggesting that a latent cofilin-dephosphorylation mechanism may also be involved in re-sequestering cofilin into rods. We were therefore interested in determining whether CIN depletion influenced cofilin rod disassembly and/or persistent rod reformation after ATP-repletion (24 hours).

Cortical neurons assembled and diassembled cofilin rods with remarkable plasticity during ATP depletion and repletion (Figure S7B); the abundance of cofilin rods and proportion of rod-forming cells increased more than 10-fold over untreated neurons 30 min. following ATP depletion. Consequent repletion of ATP for 1h resulted in the disassembly of cofilin rods to background levels, and prolonged incubation in ATP-repletion media (24h) resulted in the reappearance of persistent cofilin rods in 39% of neurons scored. We compared cofilin rod assembly, disassembly and reassembly profiles between control and CIN-depleted cortical neurons (Figure S7C): CIN depletion only appeared to influence initial cofilin rod-formation 30 min. following ATP depletion, and had very little effect on the disappearance of rods during short-term (20 min. and 1h) or reappearance of rods with long-term (24 h) ATP-repletion (Figure S7C). Similar to previous observations, we found very few inviable neurons by trypan blue staining throughout the ATP depletion and consequent repletion regimen (Minamide et al., 2000) (Supplementary Figure S7D). Furthermore, CIN depletion had no additive effects on cell viability compared to control-depleted neurons (Supplementary Figure S7D).

We next determined whether 17AAG could induce cofilin dephosphorylation and rod formation in neurons. 5 μM 17AAG induced cofilin dephosphorylation (Figure S8A) and optimal cofilin rod formation (Figure S8B and C) in cultured cortical neurons without any significant influence on CIN protein stability (Figure S8A). Neurons required incubation with higher 17AAG concentrations for cofilin rod formation (5 μM for 16h) (Figure S8C), in comparison to 2 μM for 8h in cofilin-GFP HeLa cells (Figure 5A). CIN expression levels are unlikely to explain the heightened sensitivity to 17AAG in HeLa cells, as there was little difference from CIN expression in bovine brain cytosol. In contrast, Hsp90 levels are more abundant in HeLa lysates by over three-fold compared to brain lysates (Figure S9). This difference in Hsp90 expression likely renders HeLa cells more sensitive to 17AAG-triggered cofilin dephosphorylation compared to primary neurons.

Treatment of both hippocampal and cortical neurons with 5 μM 17AAG resulted in the formation of cofilin rods (Figure 7A). As in HeLa cells, CIN depletion resulted in the suppression of 17AAG-induced phosphocofilin turnover in cortical neurons (Figure 7B), and cofilin rod formation in hippocampal neurons (Figure 7C). Together, these results implicate a general role for CIN in mediating p-cofilin turnover and consequent rod formation during energy stress in neurons.

Discussion

Our results indicate a mechanism whereby ATP depletion results in enhanced CIN-dependent cofilin dephosphorylation and rod formation as a result of attenuated Hsp90 interactions (Figure 7D). One consequence of the Hsp90/CIN-dependent energy depletion response mechanism described here would be to dephosphorylate cofilin and sequester it into rods, thereby slowing the rate of ATP drain through the immobilization of cofilin and actin during neuronal ATP stress (Bernstein and Bamburg, 2003; Bernstein et al., 2006). CIN depletion alone, however, is insufficient to abrogate p-cofilin turnover entirely during ATP depletion, suggesting that multiple cofilin signaling components may be regulated during energy stress. In support of this notion, we also observe delayed p-cofilin turnover with siRNA depletion of the cofilin phosphatase SSH-1L (Figure S2B), and rapid dephosphorylation of the cofilin kinase, LIMK1, within the kinase activation loop (T508) between 2 to 10 min following ATP depletion (Figure S10). These results suggest that cofilin dephosphorylation integrates both kinase-inactivating and phosphatase-activating mechanisms during energy depletion.

Although the human brain only accounts for approximately 2% of the total body mass, up to 20% of the metabolic expenditure is disproportionately reserved for neuronal function (Attwell and Laughlin, 2001). The heavy energy load of neural tissue also renders it sensitive to fluctuations in energy production resulting from perturbations in glycolytic or oxidative respiration pathways. Microischemic episodes due to vascular dysfunction or stroke could potentially increase the risk for developing pathological and cognitive phenotypes associated with Alzheimer's disease (AD) (Kalaria, 2000). Indeed, loss of cytoplasmic ATP is an early consequence of mitochondrial dysfunction and can result in the pathological manifestation of AD and Parkinson's disease (Andersen, 2004).

It is still unclear how cells sense the availability of ATP with respect to neurodegeneration. However, since ATP has been shown to be an integral part of cellular Hsp90 function (Obermann et al., 1998; Panaretou et al., 1998), it is reasonable that Hsp90 may have a role in transducing ATP availability to downstream signaling machinery. Interestingly, the Hsp90 inhibitor 17AAG ameliorates motor defects in a neurodegenerative mouse model of spinal and bulbar muscular atrophy (Waza et al., 2005), while geldanamycin reduces neurotoxic α-synuclein aggregates in *Drosophila* models (Auluck et al., 2005) and provides neuroprotection in a chemically-induced Parkinson's Disease mouse model (Shen et al., 2005). Geldanamycin

also limits neuronal damage during surgically-induced cerebral ischemia in rats (Lu et al., 2002). Thus, perturbation of ATP-dependent Hsp90 function appears to confer neuroprotection.

Under normal physiological circumstances, regulated cofilin activity is required for neuronal migration during early development of the cerebral cortex (Bellenchi et al., 2007), neurite extension (Meberg and Bamburg, 2000), axonogenesis (Garvalov et al., 2007) and growth cone steering (Wen et al., 2007). Neurodegenerative stress, however, coincides with the formation of large filamentous rod-shaped cofilin/actin inclusions in brains of patients afflicted with AD (Minamide et al., 2000). Rod-shaped cofilin/actin aggregates are also formed in response to amyloid β peptides and in transgenic AD mice (Maloney et al., 2005), as well as in tau-induced neurodegenerative mouse and *Drosophila* models (Fulga et al., 2007), demonstrating that pathological rod formation is a common feature of neurodegenerative systems. Our preliminary studies have found that the CIN-Hsp90-regulatory mechanism also appears to be critical for amyloid β-induced cofilin/actin rod formation (I Marsden, LM, TYH, GMB, and JRB - unpublished results).

It is reasonable to speculate that chronic persistence of large cofilin aggregates would have a detrimental impact on proper neuronal function. In support of this notion, cofilin/actin rod formation in *Aplysia* neurons was observed to disrupt synaptic structure and transmission (Jang et al., 2005). Rods also block vesicular transport, causing the accumulation at rods of amyloid precursor protein (APP), its processing enzymes, and β secretase-cleaved APP (Maloney et al., 2005). Soluble forms of amyloid β induce rapid cofilin/actin rod formation, suggesting a potential mechanism for propagating the region of neural dysfunction (Maloney et al., 2005). Both the short-term and long-term effects of rod formation were observed in the absence of appreciable cell death (Jang et al., 2005; Minamide et al., 2000). Whether rod formation produces any effects on long-term neuronal survival will require further study in appropriate model systems.

CIN is abundantly expressed in other tissues that are sensitive to ischemic injury (e.g. kidney) and in tissues that exhibit elevated ATP turnover (e.g. skeletal muscle, heart) (Gohla et al., 2005). This implies that an Hsp90/CIN energy-sensitive cofilin activation mechanism may be involved in consequent actin reorganization during ATP stress in these tissues. Indeed, cofilin dephosphorylation during ischemic stress has been implicated in actin disassembly and the characteristic changes in vascular permeability of non-neuronal cell types (Schwartz et al., 1999; Suurna et al., 2006). Thus, in cell types unable to form cofilin rods, CIN may mediate cytoskeletal changes during energy stress. We have established the regulation of CIN activity through Hsp90 binding as a novel molecular mechanism for directly coupling ATP stress to both homeostatic and pathological changes in the actin cytoskeleton.

Methods

Cell culture and transfection

HeLa cells were cultured in DMEM supplemented with 8% FBS. HeLa cells stably expressing wild-type cofilin1-eGFP or his_6myc-CIN were obtained by transfection with pcDNA3 cofilin-eGFP or pcDNA3 his_6myc-CIN constructs using Lipofectamine-plus reagent and selecting for clonal cell-lines in 96-well plates in 500μg/ml Geneticin (Invitrogen). Primary mouse cortical or hippocampal neurons were dissected from E17 embryos obtained from pregnant C57BL/6J mice, stored in liquid nitrogen, and cultured using Neurobasal medium upon initial seeding (Mattson and Kater, 1988; Minamide et al., 2000).

HeLa cells were transfected with DNA plasmid constructs using Lipofectamine-plus reagent (Invitrogen) at approximately 70–80% confluency. Synthetic siRNA oligonucleotide duplexes

were transfected at low cell density (~30% confluency) with Lipofectamine 2000 (Invitrogen) according to manufacturer's specifications.

Antibodies and plasmid constructs

CIN polyclonal antibodies were affinity purified from rabbit antisera as described (Gohla et al., 2005). 9E10 monoclonal antibody was used to detect the myc epitope. Antibodies to GST (Santa Cruz), p-cofilin (Cell Signaling), cofilin (Cytoskeleton), Hsp90 (Stressgen), and actin (ICN) were purchased from commercial sources.

Wild-type CIN was cloned in-frame into the pRK5-GST mammalian expression vector. Wild-type human cofilin1 was cloned into pCDNA3 in-frame with C-terminal HAhis_6 or eGFP to produce pcDNA3 cofilinHAhis_6 or pcDNA3 cofilin-eGFP constructs. pCDNA3 SSH1-GST was cloned by ligating the human SSH1L sequence (kindly provided by T. Uemura) in-frame with a downstream GST sequence.

Protein purification

Hsp90 was expressed in BL21 *E. coli* transformed with a pET14b Hsp90 expression construct (kindly provided by C. Gurkan) and purified essentially as described (McLaughlin et al., 2002), where Hsp90 was dialyzed in phosphatase buffer (10mM Hepes pH 7.5, 150mM NaCl, 10mM $MgCl_2$, 5% glycerol) immediately following imidazole elution. p-Cofilin-HAhis_6 was expressed in HeLa cells, lysed in phosphatase buffer with 10 mM imidazole and 1% NP40, and precipitated with Ni-NTA agarose (Qiagen). p-Cofilin-HAhis_6 eluates were dialyzed in phosphatase buffer containing 1mM DTT overnight at 4°C, and frozen at −80°C.

NiNTA precipitation and elution of his_6myc-CIN complexes

Detergent-free cell extracts from untransfected and clonal his_6myc-CIN-expressing cell lines were generated by sonication in phosphatase buffer in the presence of protease inhibitors. Cell debris was removed by centrifugation at 10,000 x g for 10 minutes, and 10 mg of protein was incubated with 200 µl of NiNTA-agarose for 1h at 4°C in the presence of 10 mM imidazole. Precipitates were washed four times with 25 mM imidazole in phosphatase buffer, eluted in 7 ×100 µl fractions with 0.3 M imidazole, then resolved by SDS-PAGE and immunoblotted for his_6myc-CIN or Hsp90.

RNA interference

HeLa cells were transfected with CIN-specific synthetic siRNA oligo duplex (Dharmacon) sequences 5′-GCGCCGUGCUUGUGGGCUA-3′ (Oligo1) and 5′-GCACGCUUAUGGUGGGUGA-3′ (Oligo4) at a final concentration of 5 or 10 nM using Lipofectamine2000. Control siRNA oligos comprised a non-targeting siRNA pool (Dharmacon D-001206-13-20)(Gohla et al., 2005) transfected at identical concentrations and conditions. Cells were treated for biochemical analysis or processed for fluorescence microscopy 48 h after transfection. For immunoblot analysis, HeLa cells were transfected with the siRNA Oligo 1 sequence in comparison to the non-targeting control.

The pCDNA3 mRFP/H1-shRNA used to co-express mRFP and hairpin RNA sequences were generated by cloning mRFP downstream of the pCDNA3 CMV promoter, while the H1 promoter was cloned into a distal single BglII site. Two CIN targeting sequences corresponding to CIN synthetic oligo1 and 4 sequences described above, and the non-targeting (NT) sequence 5' GCGCGCTATGTAGGATTCG 3' were converted to shRNA hairpin sequences and cloned behind the H1 promoter.

Mouse cortical and hippocampal neurons were tandemly transfected using synthetic non-targeting control or mouse PDXP siRNA oligo pools (Dharmacon L-040273-01-0005) at DIV3

and DIV5 at a concentration of 10 nM using RNAi Max transfection agent (Invitrogen). Cells were then treated for biochemical analysis or processed for immunofluorescence analysis at DIV7.

ATP depletion

ATP was depleted in HeLa cells using either 0.2 μM antimycinA (Sigma) or 10 mM NaN_3/6 mM 2-deoxyglucose in DMEM medium lacking glucose (Invitrogen) or in PBS for mouse primary neuronal cultures as described (Minamide et al., 2000).

Phosphatase assays

Cofilin dephosphorylation by GST or GST-CIN precipitates was measured *in vitro* using a *p*-cofilin-HAhis_6 substrate purified from HeLa cells. GST or GST-CIN expressed in HeLa cells were precipitated using glutathione sepharose in phosphatase buffer with 1% NP40, and washed extensively. Precipitates were then incubated with purified p-cofilin-HAhis_6 with or without purified Hsp90 in phosphatase buffer for 1.5 h at 37°C, and reactions stopped by addition of sample buffer and boiling. p-Cofilin dephosphorylation was determined by the disappearance of p-cofilin detected by immunoblotting using a phospho-specific antibody recognizing p-cofilin. Blots were stripped and reprobed with an anti-HA antibody to determine total cofilin in the assays, and p-cofilin levels were normalized for total cofilin by densitometric analysis.

Fluorescence imaging

Cofilin-GFP was visualized in HeLa cells seeded on glass coverslips by fixation in 4% paraformaldehyde at room temperature for 45 min, followed by extraction in cold methanol for 3 min, then washing in PBS and mounting on glass slides in anti-fade reagent (Prolong Gold, Molecular Probes).

Visualization of cofilin-GFP rod formation in live cells stably expressing cofilin-GFP was undertaken on a heated stage (37°C). Cofilin-GFP cells were transfected with shRNA vectors described above for 48 hours, and subsequently re-seeded with untransfected cofilin-GFP cells. shRNA-transfected and non-transfected co-cultures were incubated overnight, and ATP-depleted using NaN_3/2-deoxyglucose in glucose-free DMEM for 30 min. Fluorescence images were obtained every 15 s for a total of 30 min, and shRNA-expressing cells were marked by RFP fluorescence during image analysis. Primary murine hippocampal cultures were fixed and stained for cofilin and actin using specific poly or monoclonal antibodies respectively, and visualized after detection with fluorescent secondary antibodies.

Statistical analyses

All statistical analyses presented were calculated using two-tailed Student’s t-tests.

Supplementary Material

Refer to Web version on PubMed Central for supplementary material.

Acknowledgements

The authors thank Bruce Fowler and Ben Bohl for technical assistance. Special thanks to Drs. Paul LaPointe, Cemal Gurkan, Joerg Birkenfeld, Alisa Piekny, Madelaine Lancaster, Antje Gohla and Céline DerMardirossian for helpful discussion. This work was supported by NIH grants GM44428 (to GMB) and NS40371 (to JRB). TYH was supported by a postdoctoral fellowship from the American Heart Association; JRB was supported in part by a sabbatical leave from Colorado State University.

References

Agnew BJ, Minamide LS, Bamburg JR. Reactivation of phosphorylated actin depolymerizing factor and identification of the regulatory site. The Journal of biological chemistry 1995;270:17582–17587. [PubMed: 7615564]

Attwell D, Laughlin SB. An energy budget for signaling in the grey matter of the brain. J Cereb Blood Flow Metab 2001;21:1133–1145. [PubMed: 11598490]

Auluck PK, Meulener MC, Bonini NM. Mechanisms of Suppression of {alpha}-Synuclein Neurotoxicity by Geldanamycin in Drosophila. The Journal of biological chemistry 2005;280:2873–2878. [PubMed: 15556931]

Bellenchi GC, Gurniak CB, Perlas E, Middei S, Ammassari-Teule M, Witke W. N-cofilin is associated with neuronal migration disorders and cell cycle control in the cerebral cortex. Genes Dev 2007;21:2347–2357. [PubMed: 17875668]

Bernstein BW, Bamburg JR. Actin-ATP hydrolysis is a major energy drain for neurons. J Neurosci 2003;23:1–6. [PubMed: 12514193]

Bernstein BW, Chen H, Boyle JA, Bamburg JR. Formation of actin-ADF/cofilin rods transiently retards decline of mitochondrial potential and ATP in stressed neurons. American journal of physiology 2006;291:C828–C839. [PubMed: 16738008]

Carlier MF, Laurent V, Santolini J, Melki R, Didry D, Xia GX, Hong Y, Chua NH, Pantaloni D. Actin depolymerizing factor (ADF/cofilin) enhances the rate of filament turnover: implication in actin-based motility. The Journal of cell biology 1997;136:1307–1322. [PubMed: 9087445]

Fulga TA, Elson-Schwab I, Khurana V, Steinhilb ML, Spires TL, Hyman BT, Feany MB. Abnormal bundling and accumulation of F-actin mediates tau-induced neuronal degeneration in vivo. Nature cell biology 2007;9:139–148.

Garvalov BK, Flynn KC, Neukirchen D, Meyn L, Teusch N, Wu X, Brakebusch C, Bamburg JR, Bradke F. Cdc42 regulates cofilin during the establishment of neuronal polarity. J Neurosci 2007;27:13117–13129. [PubMed: 18045906]

Gohla A, Birkenfeld J, Bokoch GM. Chronophin, a novel HAD-type serine protein phosphatase, regulates cofilin-dependent actin dynamics. Nature cell biology 2005;7:21–29.

Grenert JP, Sullivan WP, Fadden P, Haystead TA, Clark J, Mimnaugh E, Krutzsch H, Ochel HJ, Schulte TW, Sausville E, et al. The amino-terminal domain of heat shock protein 90 (hsp90) that binds geldanamycin is an ATP/ADP switch domain that regulates hsp90 conformation. The Journal of biological chemistry 1997;272:23843–23850. [PubMed: 9295332]

Ichetovkin I, Grant W, Condeelis J. Cofilin produces newly polymerized actin filaments that are preferred for dendritic nucleation by the Arp2/3 complex. Curr Biol 2002;12:79–84. [PubMed: 11790308]

Jang DH, Han JH, Lee SH, Lee YS, Park H, Lee SH, Kim H, Kaang BK. Cofilin expression induces cofilin-actin rod formation and disrupts synaptic structure and function in Aplysia synapses. Proceedings of the National Academy of Sciences of the United States of America 2005;102:16072–16077. [PubMed: 16247020]

Kalaria RN. The role of cerebral ischemia in Alzheimer's disease. Neurobiology of aging 2000;21:321–330. [PubMed: 10867217]

Lu A, Ran R, Parmentier-Batteur S, Nee A, Sharp FR. Geldanamycin induces heat shock proteins in brain and protects against focal cerebral ischemia. J Neurochem 2002;81:355–364. [PubMed: 12064483]

Maloney MT, Bamburg JR. Cofilin-mediated neurodegeneration in Alzheimer's disease and other amyloidopathies. Molecular neurobiology 2007;35:21–44. [PubMed: 17519504]

Maloney MT, Minamide LS, Kinley AW, Boyle JA, Bamburg JR. Beta-secretase-cleaved amyloid precursor protein accumulates at actin inclusions induced in neurons by stress or amyloid beta: a feedforward mechanism for Alzheimer's disease. J Neurosci 2005;25:11313–11321. [PubMed: 16339026]

Mattson MP, Kater SB. Isolated hippocampal neurons in cryopreserved long-term cultures: development of neuroarchitecture and sensitivity to NMDA. Int J Dev Neurosci 1988;6:439–452. [PubMed: 2849287]

McLaughlin SH, Smith HW, Jackson SE. Stimulation of the weak ATPase activity of human hsp90 by a client protein. Journal of molecular biology 2002;315:787–798. [PubMed: 11812147]

Meberg PJ, Bamburg JR. Increase in neurite outgrowth mediated by overexpression of actin depolymerizing factor. J Neurosci 2000;20:2459–2469. [PubMed: 10729326]

Minamide LS, Striegl AM, Boyle JA, Meberg PJ, Bamburg JR. Neurodegenerative stimuli induce persistent ADF/cofilin-actin rods that disrupt distal neurite function. Nature cell biology 2000;2:628–636.

Niwa R, Nagata-Ohashi K, Takeichi M, Mizuno K, Uemura T. Control of actin reorganization by Slingshot, a family of phosphatases that dephosphorylate ADF/cofilin. Cell 2002;108:233–246. [PubMed: 11832213]

Obermann WM, Sondermann H, Russo AA, Pavletich NP, Hartl FU. In vivo function of Hsp90 is dependent on ATP binding and ATP hydrolysis. The Journal of cell biology 1998;143:901–910. [PubMed: 9817749]

Panaretou B, Prodromou C, Roe SM, O'Brien R, Ladbury JE, Piper PW, Pearl LH. ATP binding and hydrolysis are essential to the function of the Hsp90 molecular chaperone in vivo. Embo J 1998;17:4829–4836. [PubMed: 9707442]

Pearl LH, Prodromou C. Structure and mechanism of the Hsp90 molecular chaperone machinery. Annual review of biochemistry 2006;75:271–294.

Pollard TD, Borisy GG. Cellular motility driven by assembly and disassembly of actin filaments. Cell 2003;112:453–465. [PubMed: 12600310]

Schwartz N, Hosford M, Sandoval RM, Wagner MC, Atkinson SJ, Bamburg J, Molitoris BA. Ischemia activates actin depolymerizing factor: role in proximal tubule microvillar actin alterations. The American journal of physiology 1999;276:F544–F551. [PubMed: 10198413]

Shen HY, He JC, Wang Y, Huang QY, Chen JF. Geldanamycin induces heat shock protein 70 and protects against MPTP-induced dopaminergic neurotoxicity in mice. The Journal of biological chemistry 2005;280:39962–39969. [PubMed: 16210323]

Smith DF, Stensgard BA, Welch WJ, Toft DO. Assembly of progesterone receptor with heat shock proteins and receptor activation are ATP mediated events. The Journal of biological chemistry 1992;267:1350–1356. [PubMed: 1730655]

Suurna MV, Ashworth SL, Hosford M, Sandoval RM, Wean SE, Shah BM, Bamburg JR, Molitoris BA. Cofilin mediates ATP depletion-induced endothelial cell actin alterations. Am J Physiol Renal Physiol 2006;290:F1398–F1407. [PubMed: 16434575]

Waza M, Adachi H, Katsuno M, Minamiyama M, Sang C, Tanaka F, Inukai A, Doyu M, Sobue G. 17-AAG, an Hsp90 inhibitor, ameliorates polyglutamine-mediated motor neuron degeneration. Nature medicine 2005;11:1088–1095.

Wen Z, Han L, Bamburg JR, Shim S, Ming GL, Zheng JQ. BMP gradients steer nerve growth cones by a balancing act of LIM kinase and Slingshot phosphatase on ADF/cofilin. The Journal of cell biology 2007;178:107–119. [PubMed: 17606869]

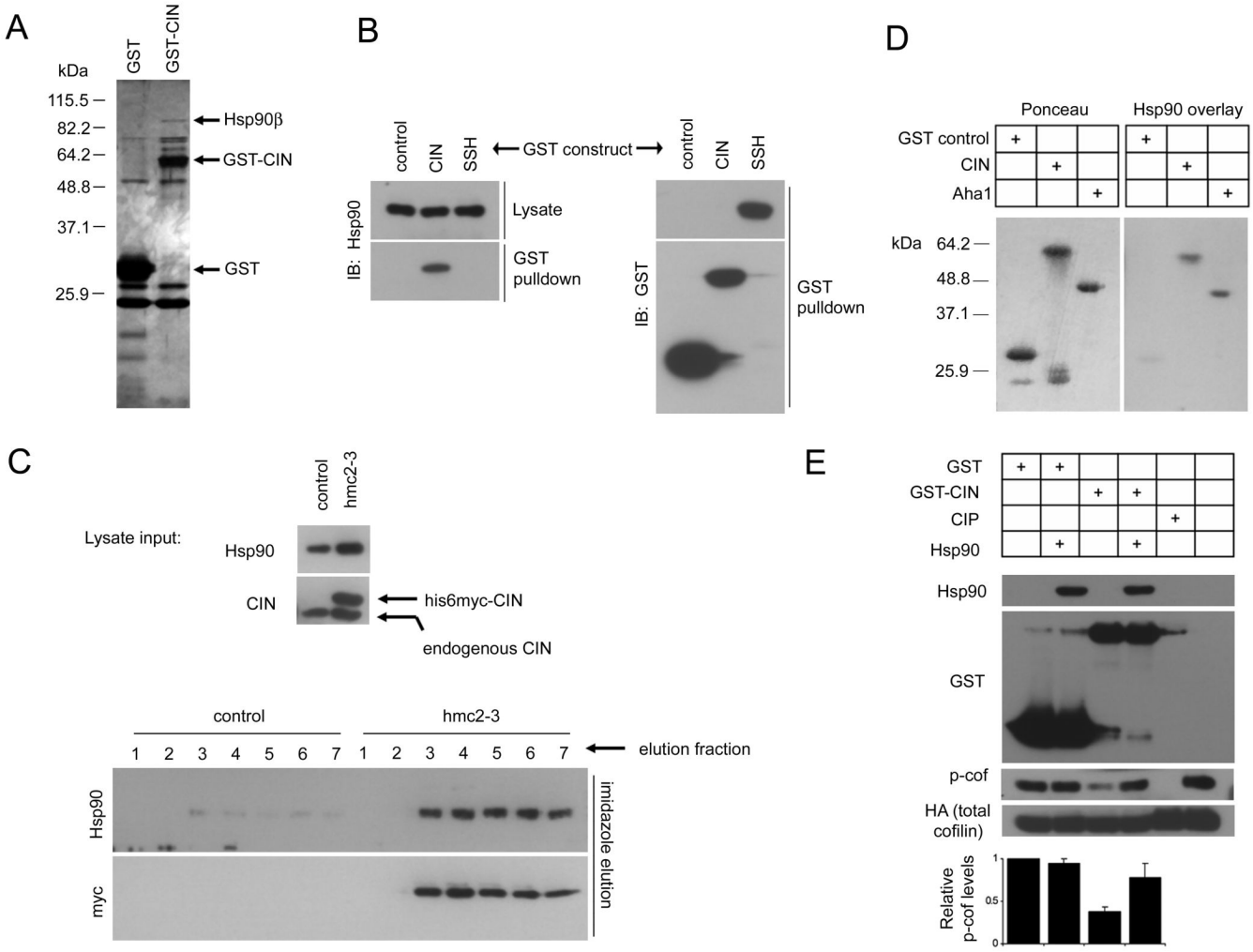

Figure 1. The molecular chaperone Hsp90β interacts with CIN

(A) GST or GST-CIN complexes were precipitated from HeLa cell lysates, resolved by SDS-PAGE, and silver stained. Co-elution of GST-CIN with a ~90kDa band, subsequently identified by mass spectrometry as Hsp90β, was observed. (B) HeLa cells expressing GST alone (control), GST-CIN or SSH-GST were precipitated with glutathione sepharose, then immunoblotted for Hsp90 or GST-tagged constructs, as indicated. (C) His-tagged proteins were precipitated, eluted and immunoblotted from control and clonal his_6myc-CIN expressors (hmc2–3) as described in Methods. (D) Purified GST, GST-CIN, and Aha1 proteins were transferred onto nitrocellulose and visualized by Ponceau S staining. The blot was then overlaid with 3.3 μg of purified Hsp90β for 2 h at room temperature, and bound Hsp90β detected by immunoblot. The results shown are representative of two experiments. (E) Hsp90 inhibits CIN phosphatase activity *in vitro*. GST and GST-CIN precipitates were assayed for phosphatase activity using purified p-cofilin as in Methods. A calf intestinal phosphatase (CIP) positive control is included. The bar graph represents p-cofilin levels normalized to total cofilin levels, where p-cofilin levels are set at 1.0 in GST control precipitates (mean +/− SEM in three independent experiments).

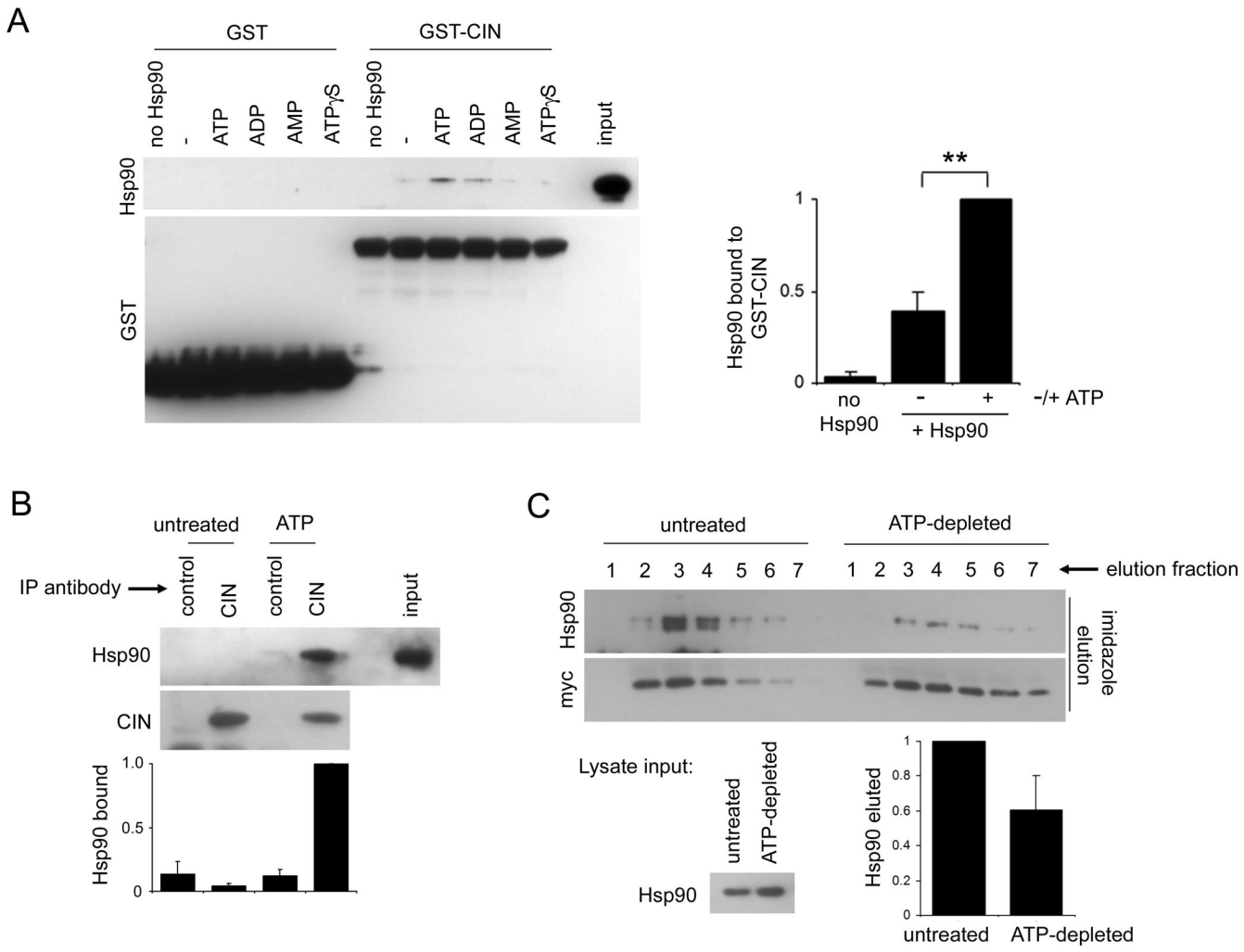

Figure 2. ATP enhances interactions between Hsp90 and CIN

(A) GST and GST-CIN immobilized on glutathione sepharose was incubated in the presence or absence of recombinant Hsp90 +/− 5 mM of various adenosine nucleotides. The graph depicts Hsp90β co-precipitation with GST-CIN beads, with Hsp90β-binding in the presence of ATP set at 1.0 (mean +/− SEM in four independent assays). ATP consistently enhanced CIN/Hsp90β coprecipitation (**p<0.02). (B) ATP facilitates CIN/Hsp90 complex formation in brain extracts. 250 μg bovine brain extract was immunoprecipitated with 1 μg control, or affinity-purified CIN antibodies/protein G sepharose in the absence (untreated) or presence of 5mM ATP. 2 μg of brain extract input is shown. The graph below depicts average Hsp90 intensities from 3 independent experiments +/− SEM (where the highest Hsp90 measurement is set to 1.0). (C) ATP depletion attenuates CIN/Hsp90 interactions *in vivo*. his_6myc-CIN was precipitated from detergent-free hmc2–3 cell lysates from untreated cells or cells subjected to ATP depletion for 30 min with 0.2 μM antimycin A. 0.3 M imidazole elution fractions were immunoblotted for Hsp90 and his_6myc-CIN. 10 μg of lysate was immunoblotted for Hsp90. Densitometric measurement of Hsp90 eluates normalized against CIN eluates and Hsp90 levels in the input lysate revealed a 40% reduction in Hsp90 co-elution upon ATP depletion (bar graph; average and SEM derived from three experiments is shown).

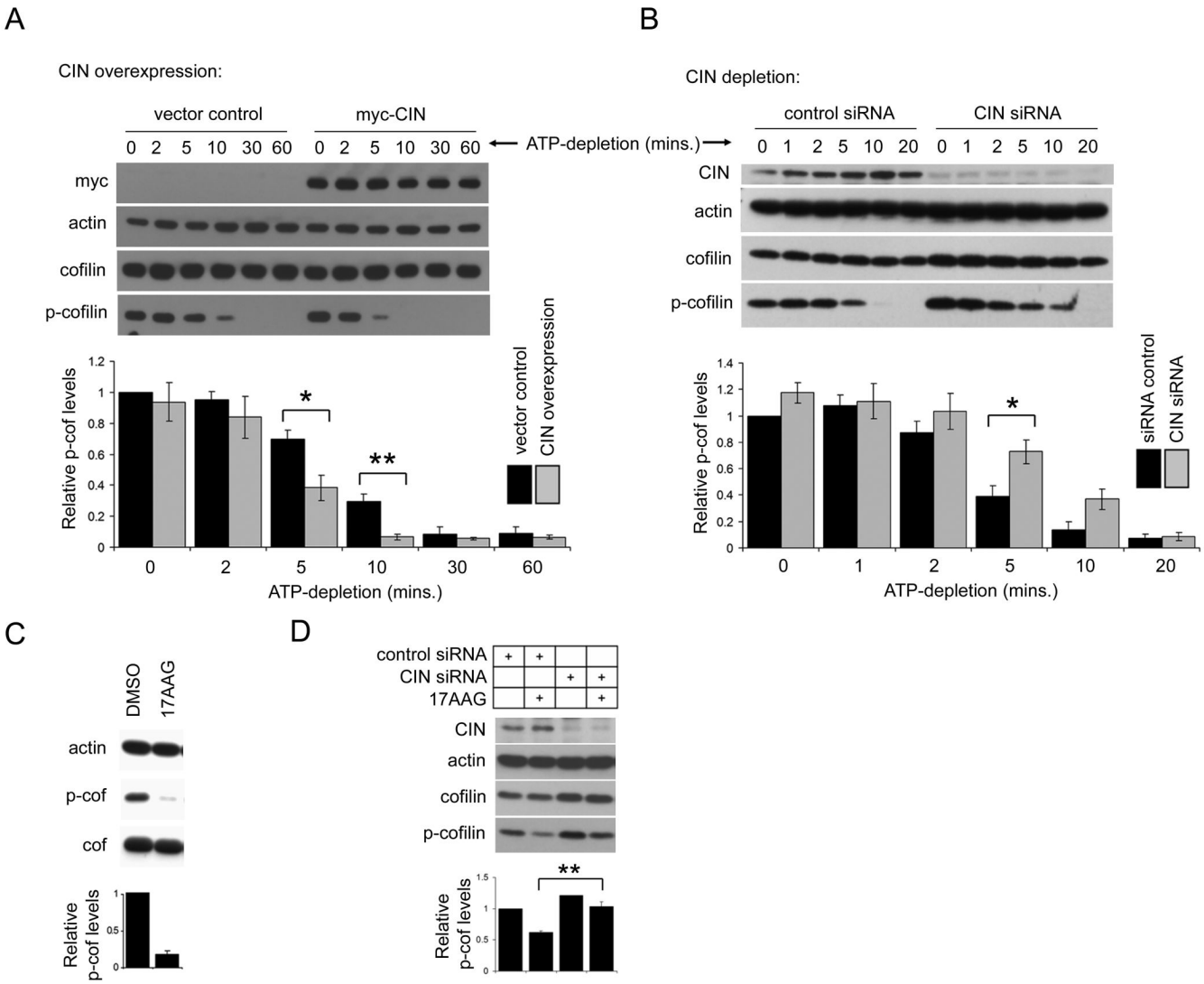

Figure 3. CIN mediates phosphocofilin turnover during anoxic stress and Hsp90 inhibition

(A) CIN overexpression accelerates cofilin dephosphorylation during ATP depletion. HeLa cells were transfected with control vector or his_6myc-CIN (myc-CIN) and treated with 0.2 μM antimycin A for the time indicated, and phosphocofilin dephosphorylation determined. (B) CIN depletion delays phosphocofilin turnover during anoxic stress. HeLa cells transfected with CIN-targeting or control siRNA oligos were subjected to ATP depletion as above for 20 min. CIN immunoblots showed that CIN levels were reduced in the extracts 48 h after transfection. (C) 17AAG triggers cofilin dephosphorylation. Extracts from HeLa cells treated 16 h with DMSO or 1 μM 17AAG were immunoblotted as indicated. Phosphocofilin levels were normalized to total cofilin densitometrically, and set to 1.0 in DMSO treatments (bar graph presented represents mean +/− SEM in three samples). (D) 17AAG-mediated phosphocofilin dephosphorylation is CIN-dependent. Extracts from HeLa cells transfected with control or CIN siRNA oligos were incubated in the presence of 2 μM 17AAG for 5 h, and phosphocofilin levels determined by immunoblot. All graphs represent averaged p-cofilin measurements normalized against cofilin from a minimum of three experiments (+/−SEM), where statistical differences were determined by two-tailed Student's t-tests (* $p<0.05$, ** $p<0.02$)

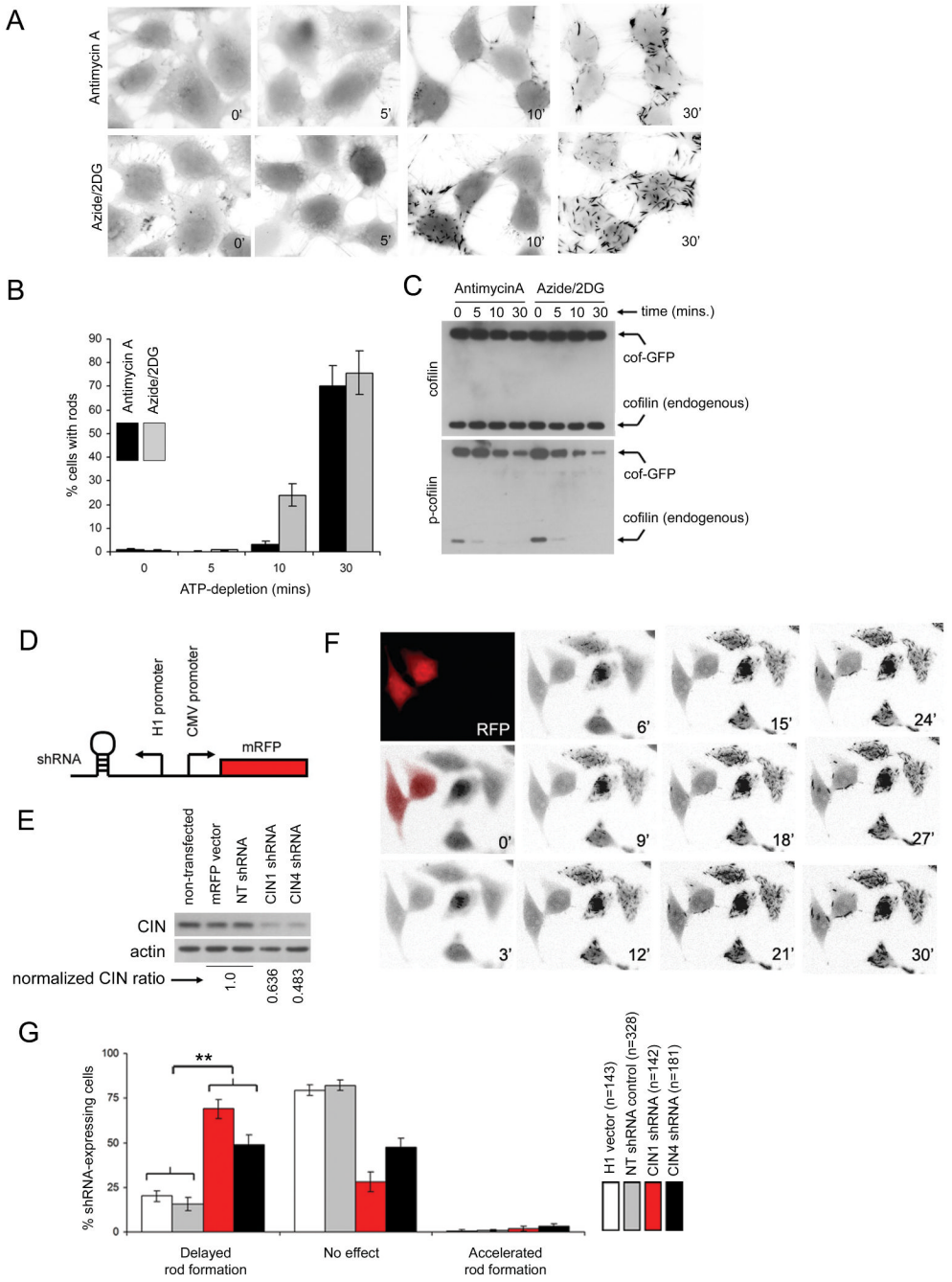

Figure 4. CIN depletion attenuates cofilin rod formation induced by ATP depletion in an engineered rod assembly system

(A) through (C), A model system for cofilin rod formation in vivo. (A) A clonal HeLa cell line expressing cofilin-GFP was subjected to ATP depletion in the presence of antimycin A or NaN_3/2-deoxyglucose (Azide/2DG) for 0, 5, 10 and 30 min and fixed for fluorescence microscopy. Cofilin-GFP rods appear as dark tapered inclusions in the inverted fluorescence images depicted. (B) Quantification of cofilin-GFP rods during ATP depletion (mean +/− SEM, four experiments). (C) Immunoblot of extracts from cofilin-GFP cells during anoxic stimulation demonstrate the rapid dephosphorylation of both the recombinant cofilin-GFP and endogenous cofilin. (D) through (G), effect of CIN depletion on cofilin rod formation. (D) A

schematic of shRNA constructs co-expressing mRFP as described in Methods. (E) Extracts from cofilin-GFP cells were transfected with shRNA vector constructs for 48 h, and immunoblotted for CIN, with actin as a control. CIN ratios (normalized to actin) compared to H1 and non-targeting controls (averaged and set as 1.0) are given below. (F) Cofilin-GFP cells transfected with a CIN-targeting shRNA construct (CIN oligo1 sequence) were co-cultured with non-transfected cofilin-GFP cells and ATP-depleted with NaN_3/2-deoxyglucose for 30 min. shRNA-expressing cells were identified by RFP fluorescence (false colored in red in the first two frames) and the formation of cofilin rods tracked by GFP-fluorescence, where images were acquired at the times indicated (min). (G) Movies of cofilin-GFP co-cultures subjected to ATP depletion for 30 min. were observed for the emergence of cofilin rods in shRNA-expressing (RFP-tagged) cells and untransfected cells, and scored for shRNA-induced delay in rod formation. Percentages of shRNA-expressing cells producing a delayed phenotype were tabulated from each movie, with a minimum of 8 movies analyzed for each treatment. Mean percentages +/− SEM between individual movies are presented, and the total number of cells scored for each treatment (n) is indicated. Percentages of cells with delayed rod formation between vector/non-targeting control and CIN-targeting (CIN1, CIN4) shRNA groups were found to be significantly different (** $p<0.002$).

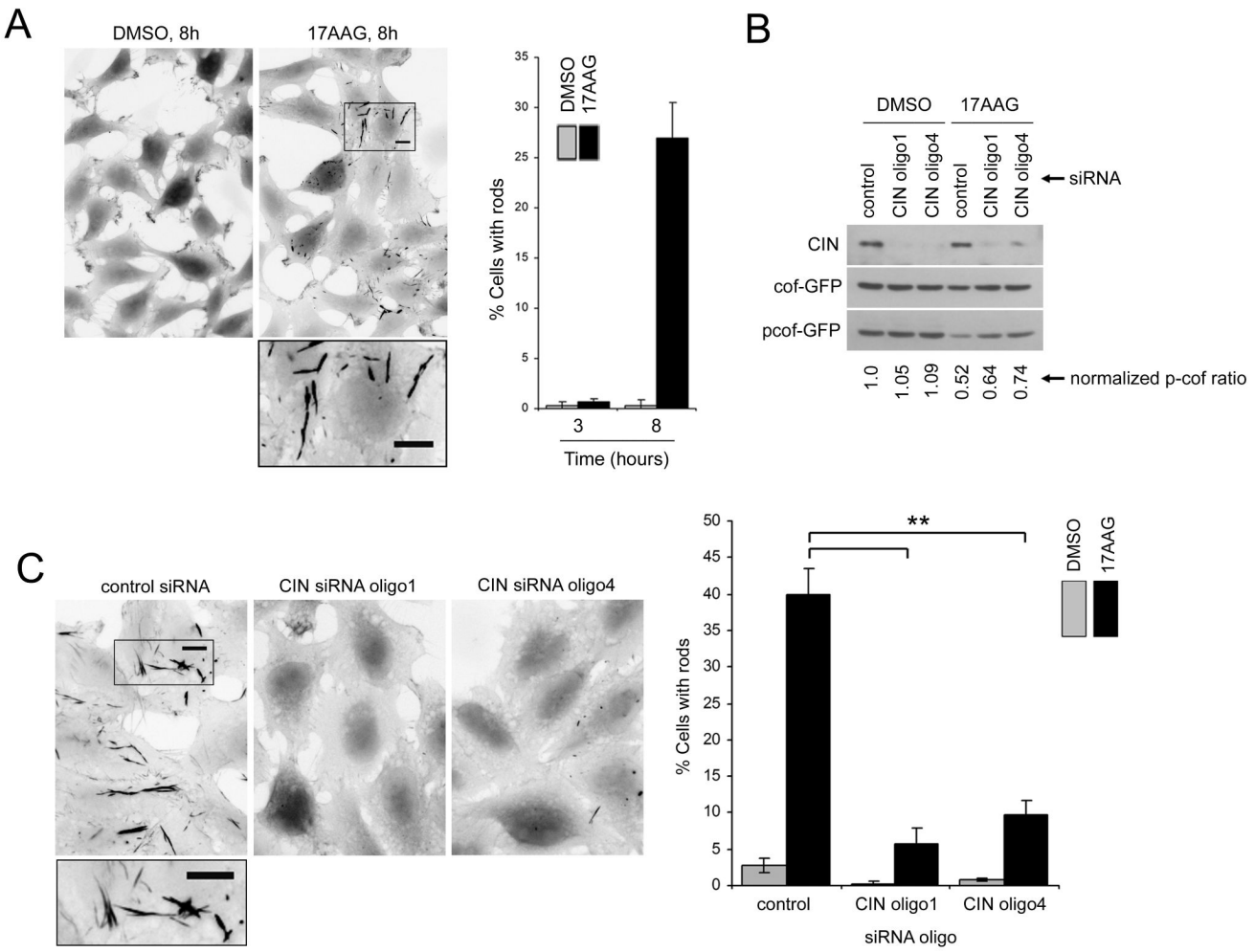

Figure 5. Hsp90 inhibition induces CIN-dependent cofilin rod formation

(A) Hsp90 inhibition induces cofilin rod formation. DMSO or 2 μM 17AAG was applied to cofilin-GFP clonal expressing cells for 3 and 8h, and fluorescent GFP images of fixed cells were scored for cofilin-GFP rod formation (mean +/− SEM, three experiments). Inverted fluorescence images reveal cofilin rods as dark inclusions with 17AAG treatment for 8 hours (a magnified image of cofilin-GFP rods is presented, scale bar = 5 μm). (B) Lysates from cofilin-GFP cells transfected with control or CIN RNAi oligos were immunoblotted to confirm CIN-depletion. Densitometric ratios determined for p-cofilin-GFP (normalized against total cofilin-GFP) are shown underneath. (C) 17AAG-mediated rod formation is CIN-dependent. Cells transfected either with control or CIN-targeting oligos (oligo1 and 4 sequences, as in Methods) were treated with 2 μM 17AAG or with DMSO for 8 h after 48 h siRNA treatment. Cells were then fixed (as in Methods) and cofilin-GFP rod formation observed using GFP fluorescence (17AAG-treated cells are displayed as inverted fluorescence images, magnified view of 17AAG-induced cofilin-GFP rods is shown, bar = 5 μm). The graph represents cells scored for rod-formation, where mean percentages (+/−SEM) were calculated from four experiments. A minimum of n=624 cells were scored for each treatment, and significant differences were observed between 17AAG-treated control and CIN-depleted groups (**p<0.0005).

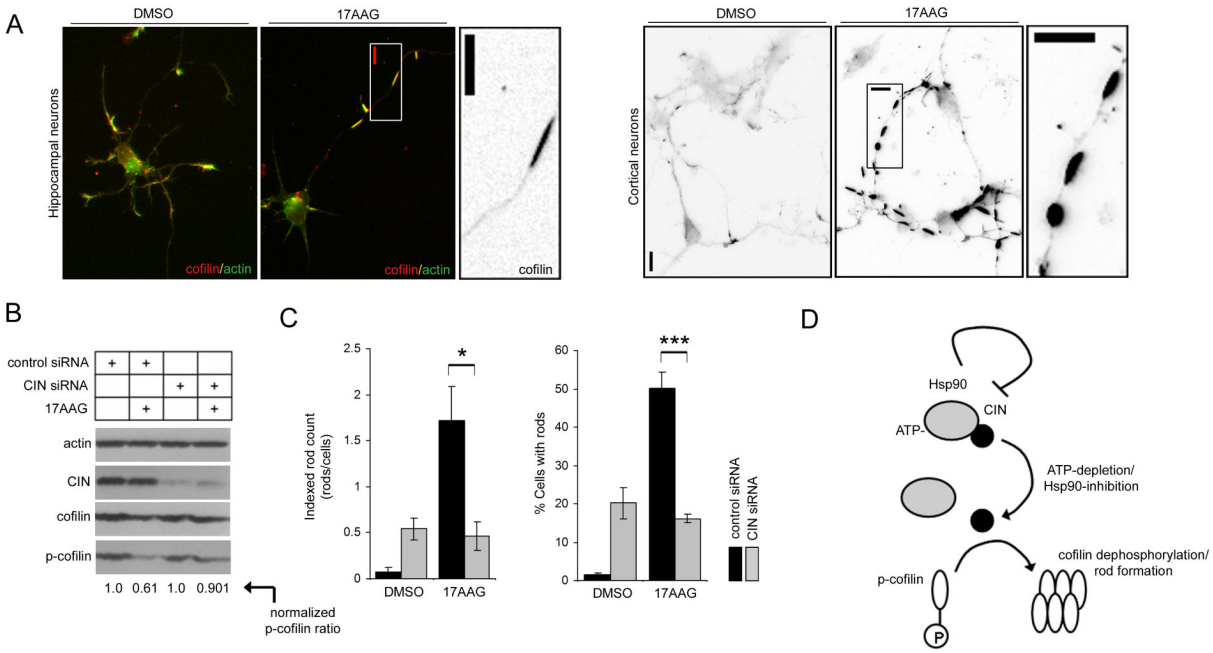

Figure 6. CIN depletion attenuates rod formation in primary neurons

(A) DIV5 primary mouse hippocampal neurons seeded on glass coverslips were left untreated or treated with NaN_3/2-deoxyglucose for 30 min (ATP depletion), and immunostained for actin (green) and cofilin (red) as described in Methods. DIV3 cortical neurons were similarly ATP-depleted for 0, 15 or 30 mins. and immunostained for cofilin (in inverted fluorescence images, rods appear dark). Magnified images are inverted fluorescence images derived from cofilin immunostaining (scale bar = 10μm). (B) Depletion of murine CIN in cortical neurons. DIV3 murine cortical neuron cultures were transfected with control or mouse CIN siRNA oligos at a final concentration of 5 or 10 nM as described in Methods. Cell lysates harvested at DIV7 were immunoblotted for CIN and Hsp90. Effectual CIN-depletion was attained by tandemly transfecting CIN-targeting oligos at a final concentration of 10 nM (graph depicts mean +/− SEM CIN levels normalized against Hsp90 averaged over 4 independent experiments). (C) CIN depletion delays cofilin dephosphorylation during ATP depletion in cortical neurons. Cortical neurons were transfected with control or CIN siRNA oligos, and treated with antimycin A for the time indicated. Cell lysates were then subject to immunoblotting. (D) siRNA transfected hippocampal neurons were subjected to ATP depletion using NaN_3/2-deoxyglucose for the time indicated, fixed and immunostained for cofilin. The percentage of rod-forming neurons was scored (left) in addition to the total number of rods counted indexed over total cells (rod index, right) for control (black line) and CIN-siRNA transfected cells (gray line). The average +/− SEM of three experiments is presented, where a minimum of 149 cells were scored for each timepoint. (E) Hippocampal neurons treated with control or CIN-targeting siRNA oligos were ATP-depleted (NaN_3/2-deoxyglucose for 0.5h), and scored for the number of cofilin rods formed indexed over cell number (left bar graph), or percentage of cell forming cells (right bar graph). Mean values over a minimum of three experiments (+/−SEM) were calculated, and differences in rod-induction between control and CIN-depleted neurons were measured by two-tailed Student's t-tests (**p<0.02, ***p<0.01), where a minimum of 342 cells were scored in total for each treatment.

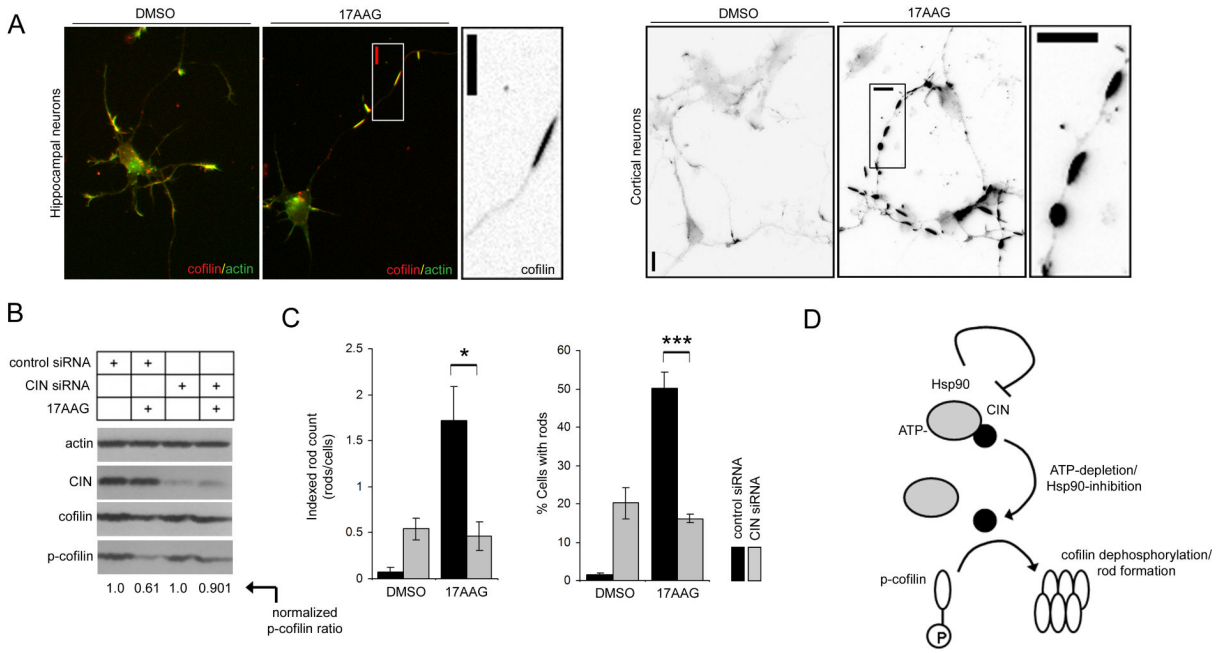

Figure 7. 17AAG induces p-cofilin turnover and CIN-dependent cofilin rod formation in neurons

(A) DIV3 hippocampal or cortical neurons were treated with 5μM 17AAG or DMSO and fixed as described in Methods. Hippocampal neurons were immunostained for cofilin and actin, and cortical neurons were immunostained for cofilin alone. In negative fluorescence images, cofilin appears as dark rods. (B) DIV6 cortical neurons transfected with control or CIN siRNA (see Methods) were treated with 5μM 17AAG or DMSO (16h), and lysates were subjected to immunoblotting on DIV7. Normalized phosphocofilin ratios determined densitometrically are shown below. (C) Control (black bars) or CIN-siRNA (gray bars) depleted hippocampal neurons were treated with 5μM 17AAG or DMSO as in (B) and immunostained for cofilin on DIV7. Neurons were scored for total rods indexed against total cell number (left graph), or percentage of rod-forming cells. A minimum of 147 cells were scored for each treatment, and significance values were evaluated using two-tailed Student's t-tests (*$p<0.05$, ***$p<0.01$). (D) A model for ATP-dependent CIN regulation. Interactions between CIN and Hsp90 are normally enhanced by physiological ATP concentrations, where CIN activity is limited by Hsp90 interaction. ATP depletion (or Hsp90 inhibition with 17AAG) results in attenuated complexation, resulting in increased CIN-mediated phosphocofilin turnover. This in turn facilitates the assembly of cofilin and actin into rod-shaped inclusions.